DEPP1: A prognostic biomarker linked to stroma-rich and immunosuppressive microenvironment, promoting oxaliplatin resistance in gastric cancer

XUDONG QIU[1*], TAO PAN[1*], TIAN KUANG[1*], YANYING SHEN[2], YIHAN ZHENG[1], HAIGANG GENG[1], BO NI[1], XIANG XIA[1], CHUNCHAO ZHU[1], ZIZHEN ZHANG[1], HUI CAO[1] and LIN TU[1]

[1]Department of Gastrointestinal Surgery, Renji Hospital, School of Medicine, Shanghai Jiao Tong University, Shanghai 200127, P.R. China; [2]Department of Pathology, Renji Hospital, School of Medicine, Shanghai Jiao Tong University, Shanghai 200127, P.R. China

Received August 09, 2024; Accepted April 15, 2025

DOI: 10.3892/or.2025.8915

Abstract. Decidual protein induced by progesterone (DEPP1) was identified to exert heterogeneous functions in several cancers, whereas its role in gastric cancer (GC) remains elusive. In the present study, differential expression analysis was conducted using three Gene Expression Omnibus datasets (GSE54129, GSE26942 and GSE3438). Validation of DEPP1 expression was performed using reverse transcription-quantitative PCR, western blotting and immunofluorescence. Kaplan-Meier survival and Cox regression analyses were employed to assess the association between DEPP1 expression and the prognosis of patients with GC. Immune infiltration analysis was conducted to explore the correlation between DEPP1 and the tumor microenvironment. The potential of DEPP1 to promote oxaliplatin resistance was assessed using flow cytometry, western blotting, and subcutaneous mouse models. DEPP1 was found to be significantly upregulated in the aforementioned cohorts, which was consistent with the clinical specimens of the present study, and it emerged as an independent risk factor for poor overall survival in patients with GC. A prognostic nomogram was developed to improve prognosis prediction. High DEPP1 expression correlated with increased infiltration of cancer-associated fibroblasts, endothelial cells, and M2 macrophages, contributing to the development of a stroma-rich and immunosuppressive microenvironment in GC. Furthermore, high DEPP1 expression was associated with reduced sensitivity to chemotherapy drugs in patients with GC. *In vitro* and *in vivo* experiments highlighted DEPP1's crucial role in promoting oxaliplatin resistance in GC. In conclusion, DEPP1 is identified as a promising prognostic biomarker linked to a stroma-rich and immunosuppressive microenvironment, and it is critical in driving oxaliplatin resistance in GC. These findings may inform personalized therapeutic strategies for patients with GC.

Correspondence to: Professor Hui Cao or Professor Lin Tu, Department of Gastrointestinal Surgery, Renji Hospital, School of Medicine, Shanghai Jiao Tong University, 160 Pu Jian Road, Pudong New District, Shanghai 200127, P.R. China
E-mail: caohuishcn@hotmail.com
E-mail: tulin@renji.com

*Contributed equally

Key words: gastric cancer, decidual protein induced by progesterone 1, prognostic biomarker, tumor microenvironment, chemotherapy resistance

Introduction

Despite a decline in incidence and mortality rates over recent decades, gastric cancer (GC) remains the 5th most common malignancy worldwide, with a significant proportion of new cases emerging in Japan, South Korea and China (1). Its asymptomatic nature in early stages often results in delayed diagnosis and increased mortality rates (2). Concurrently, there has been a burgeoning interest in elucidating the tumor microenvironment (TME) in GC progression, characterized by a complex interplay among diverse immune cells, cancer-associated fibroblasts (CAFs), endothelial cells (ECs) and various tissue-resident cells (3). This milieu undergoes dynamic changes throughout GC progression, typified by an augmented proportion of stromal and immunosuppressive cells, including CAFs, ECs and tumor-associated macrophages (TAMs) (4). Despite advancements in targeted therapy and immunotherapy, chemotherapy remains pivotal in GC treatment, notwithstanding the persistent challenge of chemotherapy resistance, the mechanisms of which remain inadequately understood (5).

Decidual protein induced by progesterone (DEPP1), initially identified as a progesterone-induced protein during decidualization of endometrial stromal cells, manifests heterogeneous roles in tumorigenesis across diverse cancers (6-10). DEPP1 contributes to cellular reactive oxygen species (ROS) accumulation in neuroblastoma by impairing catalase activity, thereby sensitizing neuroblastoma cells to ROS-induced cell death (7). DEPP1 expedites the senescence of colorectal cancer cells, characterized by the improved activity of senescence-associated β-galactosidase upon its ectopic or induced

expression, suggesting a tumor-suppressive role (8). Conversely, high DEPP1 expression is associated with a poor prognosis in patients with cervical cancer (9). In glioma, upregulated by hypoxia, DEPP1 facilitates tumor growth and predicts a poor prognosis, implicating a tumor-supportive effect (10). To the best of our knowledge, no research has explored the role of DEPP1 in GC before.

The investigation unveiled a pronounced expression of DEPP1 in GC, correlating with poor prognosis and potentially enhancing the prognostic utility of the tumor-node-metastasis (TNM) staging system. Furthermore, DEPP1 expression exhibited associations with a stroma-rich and immunosuppressive microenvironment in GC, suggesting its contributory role in shaping the TME. Notably, DEPP1 was also found to promote resistance to oxaliplatin, a commonly used chemotherapeutic agent. These findings collectively posit DEPP1 as a prognostic indicator and plausible therapeutic target for overcoming oxaliplatin resistance in GC.

Materials and methods

Data collection. Gene expression data and corresponding clinical characteristics of patients with GC were obtained from The Cancer Genome Atlas (TCGA) database [TCGA-Stomach Adenocarcinoma (STAD); https://portal.gdc.cancer.gov/] and the Gene Expression Omnibus (GEO; https://www.ncbi.nlm.nih.gov/geo/) database, including datasets GSE84437 and GSE15459 (11,12). For sequencing data from the TCGA-STAD cohort, FPKM values were transformed into transcripts per million values for subsequent analysis. Detailed clinicopathologic information for these three cohorts is summarized in Table SI. A systematic search was conducted to identify GEO datasets that provided high-quality mRNA expression profiling data for GC and normal tissues, with a minimum sample size of 50 to ensure robust statistical analysis.

Differential expression analysis. The 'limma' R package (v.3.58.1) was utilized to identify differentially expressed genes (DEGs) between GC and normal tissues in the screened GEO datasets, employing thresholds of |log2FoldChange|>0.9 and an adjusted P-value <0.05 (13). During data processing, expression values were evaluated and normalized using the 'normalizeBetweenArrays' function to ensure consistency if necessary. Subsequently, the 'VennDiagram' R package (v.1.7.3) was employed to determine the overlap of upregulated and downregulated genes across the three cohorts (14).

Cell culture and reagents. Human GC cell line MKN45 was purchased from MEISEN CELL (cat. no. CTCC-ZHYC-0503; https://www.casmart.com.cn//product-details/page/300039501/508278209). 293T cell line and GC cell line HGC27 were preserved at the Shanghai Cancer Institute (Shanghai, China). All cell lines were authenticated using short tandem repeat DNA profiling analysis and routinely tested to confirm the absence of mycoplasma contamination. MKN45 and HGC27 cells were cultured in RPMI-1640 medium (cat. no. C11875500BT; Gibco; Thermo Fisher Scientific, Inc.), supplemented with 10% fetal bovine serum (FBS) (cat. no. S711-001S; Lonsera). 293T cells were cultured in DMEM medium (C11995500BT; Gibco; Thermo Fisher Scientific, Inc.), supplemented with 10% FBS. Cultures were maintained at 37˚C in a humidified incubator with 5% CO_2. Oxaliplatin (cat. no. S1224; Selleck Chemicals) and fluorouracil (5-FU) (cat. no. HY-90006; MedChemExpress) were utilized in the present study.

RNA isolation and reverse transcription-quantitative PCR (RT-qPCR). Total RNA from 11 pairs of GC and adjacent normal tissues was extracted using the RNAsimple Total RNA Kit (cat. no. DP419; Tiangen Biotech Co., Ltd.) following the manufacturer's instructions. The concentration and quality of the isolated RNA were evaluated using a NanoDrop 2000c spectrophotometer (Thermo Fisher Scientific, Inc.), with results summarized in Table SII. Subsequently, total RNA was reverse transcribed into cDNA using the HiScript III 1st Strand cDNA Synthesis Kit (cat. no. R312; Vazyme Biotech Co., Ltd.). The RT-qPCR reaction mix was prepared according to the manufacturer instructions of ChamQ SYBR qPCR Master Mix (cat. no. Q311; Vazyme Biotech Co., Ltd.) and run on a QuantStudio Dx system (Applied Biosystems; Thermo Fisher Scientific, Inc.). First, the mix was pre-denatured at 95˚C for 5 min. Subsequently, 40 cycles were performed: 10 sec at 95˚C and 30 sec at 60˚C, followed by a melting curve analysis according to the QuantStudio's default settings. Relative mRNA expression levels were calculated using the $2^{-\Delta\Delta Cq}$ method, with GAPDH mRNA serving as an internal reference (15). The primer sequences for DEPP1 and GAPDH are provided in Table SIII.

Western blotting. GC tissues and cells underwent lysis using RIPA lysis buffer (cat. no. BL504A; Biosharp Life Sciences) supplemented with 1 mM PMSF (cat. no. ST506; Beyotime Institute of Biotechnology) on ice for 30 min. Protein concentrations were determined using a BCA Protein Quantification Kit (cat. no. 20201ES; Shanghai Yeasen Biotechnology Co., Ltd.). Subsequently, 20 μg of protein samples per lane underwent electrophoresis using 10% gel and were transferred onto 0.45-μm PVDF membranes (cat. no. IPVH00010, Sigma-Aldrich). The membranes were then incubated with 5% skimmed milk at room temperature for 1 h. Following this, the membranes were probed with primary antibodies against DEPP1 (1:1,000; cat. no. 25833-1-AP; Proteintech Group, Inc.), PARP (1:1,000; cat. no. 9532; Cell Signaling Technology, Inc.), cleaved PARP (1:500; cat. no. HY-P80448; MedChemExpress), GAPDH (1:1,000; cat. no. 5174; Cell Signaling Technology, Inc.), or β-actin (1:20,000; cat. no. 66009-1-Ig; Proteintech Group, Inc.) at 4˚C overnight, followed by incubation with peroxidase-conjugated goat anti-rabbit IgG (33101ES60, 1:5,000, Shanghai Yeasen Biotechnology Co., Ltd.) or peroxidase-conjugated goat anti-mouse IgG (1:5,000; cat. no. BL001A; Biosharp Life Sciences) at room temperature for 1 h. Finally, proteins were visualized using an Omni-ECL™ Pico Light Chemiluminescence Kit (cat. no. SQ202L; Epizyme, Inc.).

Immunofluorescence assay. GC and adjacent normal tissues were fixed with 4% paraformaldehyde at room temperature for at least 24 h. Subsequently, the formalin-fixed tissues were embedded in paraffin and sectioned into 4 μm-thick sections. The formalin-fixed and paraffin-embedded (FFPE) sections

underwent deparaffinization in xylene, followed by rehydration in an alcohol gradient, and antigen retrieval in Tris-EDTA buffer (pH 9.0). Sections were then blocked with 5% BSA (cat. no. GC305010; Wuhan Servicebio Technology Co., Ltd.) for 1 h at room temperature. Next, sections were incubated with primary antibody against DEPP1 (1:200; cat. no. NBP3-17581; Novus Biologicals, Ltd.) at 4˚C overnight, followed by incubation with secondary Alexa Fluor 594 AffiniPure Goat Anti-Rabbit IgG (1:400; cat. no. BL064A; Biosharp Life Sciences) at room temperature for 1 h in darkness. Nuclei were stained with DAPI (2 μg/ml; cat. no. G1012; Wuhan Servicebio Technology Co., Ltd.) for 10 min. Images were captured using a Nikon fluorescence microscope (ECLIPSE Ts2; Nikon Corporation).

Immunohistochemistry (IHC) assay. Human and mouse GC tissue samples were processed according to the immunofluorescence protocol up to antigen retrieval. After antigen retrieval in Tris-EDTA buffer (pH 9.0), FFPE sections were treated with 3% H_2O_2 at room temperature for 10 min to inactivate endogenous peroxidases. Sections were then blocked with 5% BSA for 1 h at room temperature. Following this, sections were incubated with primary antibody against DEPP1 (1:200; cat. no. NBP3-17581; Novus Biologicals, Ltd.), Ki67 (1:2,000; cat. no. ab15580; Abcam), or cleaved caspase 3 (1:2,000; cat. no. 9664; Cell Signaling Technology, Inc.) at 4˚C overnight, followed by incubation with Goat Anti-Rabbit IgG (1:600; cat. no. 33101ES60, 1:600; Shanghai Yeasen Biotechnology Co., Ltd.) at room temperature for 1 h. Finally, sections were subjected to a DAB Substrate Kit (cat. no. BL732A; Biosharp Life Sciences) and counterstained with hematoxylin. Images were captured using a light microscope (BX43; Olympus Corporation).

DEPP1 staining intensity and area were independently assessed by two experienced gastroenterologists, blinded to the patients' clinical characteristics. Staining intensity was graded as 0 for negative staining, 1 for weak staining, 2 for moderate staining, and 3 for intense staining. The positive staining area was rated as follows: 0 (<5%), 1 (6 to 25%), 2 (26 to 50%), 3 (51 to 75%), and 4 (>75%). Any discrepancies in assessment were resolved by consultation with a third gastroenterologist when necessary. The IHC score of DEPP1 was calculated by multiplying staining intensity by staining area, resulting in scores ranging from 0 to 12.

Construction and validation of a prognostic nomogram. Utilizing the results from multivariate Cox regression analysis in the TCGA-STAD cohort, a prognostic nomogram that integrates DEPP1 expression and clinical parameters was developed. This nomogram was constructed using the 'survival' (v.3.5-7) and 'regplot' (v.1.1) R packages (16). To evaluate its performance, calibration curves and decision curve analysis (DCA) were employed (17).

Analysis of the correlation between DEPP1 and tumor microenvironment. The stromal, immune, and estimate scores for each patient with GC in the TCGA-STAD cohort were predicted using the 'Estimation of STromal and Immune cells in MAlignant Tumor tissues using Expression data' (ESTIMATE) algorithm (18). Additionally, the EPIC, TIMER, and quanTIseq algorithms were applied to predict the infiltration level of stromal and immune cells in the GC TME based on sequencing data from the TCGA-STAD cohort by employing the 'immunedeconv' R package (v.2.1.0) (19-22).

Functional enrichment analysis and Friends analysis. Gene Ontology (GO) and Kyoto Encyclopedia of Genes and Genomes (KEGG) enrichment analyses of the DEGs between the low- and high-expression groups of DEPP1 were conducted using the 'clusterProfiler' R package (v.4.10.0) (23). Furthermore, gene set enrichment analysis (GSEA) was performed to investigate the underlying regulatory mechanisms of DEPP1 (23,24). Subsequently, Friends analysis was carried out to identify the downstream hub genes of DEPP1, with the top 10 genes with the highest GO semantic similarity designated as hub genes using the 'GOSemSim' R package (v.2.28.1) (25).

Prediction of sensitivity to chemotherapy. The half maximal inhibitory concentration (IC_{50}), a common measure reflecting tumor cell sensitivity to chemotherapy agents, was predicted using the 'oncoPredict' R package (v.1.2) (26). This prediction involved utilizing the Genomics of Drug Sensitivity in Cancer (GDSC; https://www.cancerrxgene.org/) or Cancer Therapeutics Response Portal (CTRP; https://portals.broadinstitute.org/ctrp/) dataset as a training set and the gene expression profiles from the TCGA-STAD cohort as a test set.

Lentivirus production and infection. Lentiviral plasmids encoding human DEPP1 and an empty vector were purchased from WZ Biosciences, Inc. 293T cells were transfected at 37˚C with a total of 4 μg of DEPP1-encoding plasmids, psPAX2 (cat. no. 12260; Addgene, Inc.), and pMD2.G (cat. no. 12259, Addgene, Inc.) in a ratio of 4:3:2 using jetPRIME reagent (cat. no. 114-15; Polyplus-transfection SA). After 48 h, the supernatants were collected, centrifuged, and filtered through a 0.45 um filter. The lentivirus was then transduced into GC cells in the presence of 8 μg/ml polybrene (cat. no. 40804ES76; Shanghai Yeasen Biotechnology Co., Ltd.) for 16 h. Infected cells were subsequently selected with 2 μg/ml puromycin (cat. no. ST551; Beyotime Institute of Biotechnology) for 48 h to generate stable DEPP1-expressing GC cell lines.

Cell proliferation assay. GC cells ($1x10^5$) were seeded in 12-well plates in triplicate. After 24 h, oxaliplatin was added to the culture medium to achieve a final concentration of 10 μM. Following another 24-h incubation at 37˚C, cells were harvested, and proliferation rates were assessed using the EdU Kit (cat. no. CX004; CellorLab; https://www.epizyme.cn/Products/Details/CX004) according to the manufacturer's instructions.

Annexin V/PI flow cytometry. GC cells ($1x10^5$) were seeded in 12-well plates in triplicate. Upon adherence, oxaliplatin was added to a final concentration of 20 μM. After 24 h, cells were stained with BV421-conjugated Annexin V (cat. no. 640924; BioLegend, Inc.) and PE-conjugated PI (cat. no. 421301; BioLegend, Inc.) for 15 min in the dark at room temperature. Samples were analyzed using a Cytek Northern Lights flow

cytometer (Cytek Biosciences) to detect apoptotic cells, and data were processed using FlowJo software (v.10.8.1; BD Biosciences).

Wound healing assay. GC cells ($6x10^5$) were seeded in 6-well plates in triplicate. Once confluence was reached, the cell monolayer was scratched with a sterile 200 μl pipette tip and washed three times with PBS. Cells were then cultured in serum-free RPMI 1640 medium, and images were captured at 0 and 48 h using a light microscope (Nikon ECLIPSE Ts2). Wound areas were measured using ImageJ software (1.54f; National Institutes of Health).

Animal studies. All mice were housed and fed in the specific pathogen-free animal experiment center at RenJi Hospital (Shanghai, China), where they were maintained under a controlled 12/12-h light/dark cycle, with the temperature at 23±2˚C and humidity at 50±1%. All animal experiments were conducted in accordance with institutional guidelines and were approved by the Institutional Animal Care and Use Committee of Renji Hospital (approval no. KY2021-252-B). A total of 20 female BALB/c nude mice, aged 4 weeks and weighing ~20 g, were purchased from GemPharmatech Co., Ltd. MKN45 cells ($3x10^6$), either stably expressing DEPP1 or the empty vector, were subcutaneously injected into the right flank of each mouse, with 5 mice per group. Beginning 8 days post-injection, oxaliplatin or 5% glucose saline was administered intraperitoneally at a dosage of 5 mg/kg every 2 to 4 days. Tumor volumes were measured every 2 to 4 days using the formula 0.5 x length x $width^2$. All mice were euthanized by cervical dislocation under 3% isoflurane-induced anesthesia to minimize suffering and distress when the tumor diameter reached 15 mm or when tumor burden exceeded 10% of body weight. The mice were confirmed dead by the cessation of heartbeat or breathing, or by the loss of pain response. Tumors were then harvested, weighed and subjected to further analyses.

Statistical analysis. Statistical analyses were conducted using R (v.4.1.2; https://cran.r-project.org/) or GraphPad Prism (v.8.0.1; Dotmatics) software. Continuous variables are presented as the mean ± standard deviation and compared using Wilcoxon test for two groups and Kruskal-Wallis test for three or more groups. Categorical variables are presented as counts and compared using Fisher's exact test. Pearson's correlation test was utilized to measure the correlation between two continuous variables. Logistic regression was employed to explore the correlation between DEPP1 expression and clinical features. Kaplan-Meier curves were plotted to display overall survival (OS) and disease-free survival (DFS) of patients with GC, with differences between groups determined using the log-rank test. The restricted mean survival time (RMST) difference was estimated using the 'survRM2' R package (v.1.0-4) (27). Univariate and multivariate Cox regression analyses were conducted to investigate the prognostic significance of DEPP1 and other clinicopathologic parameters. Receiver operating characteristic (ROC) curves were plotted to evaluate the ability of DEPP1 to predict the OS of patients with GC. $P<0.05$ was considered to indicate a statistically significant difference.

Results

Identification of DEPP1 as a novel upregulated gene in GC. The primary objective was to systematically identify DEGs between GC and adjacent normal tissues. A comprehensive search led to the inclusion of three GEO datasets: i) GSE54129, ii) GSE26942 and iii) GSE3438, which identified 2,786, 284 and 273 DEGs, respectively (Fig. S1; Tables SIV-SVI). Notably, DEPP1 consistently emerged as the sole upregulated gene in all three datasets, suggesting its potential significance in GC. Conversely, no genes were consistently downregulated across all datasets (Fig. 1A). Analysis of sequencing data from the TCGA-STAD dataset further corroborated these findings (Fig. 1B). To validate these results, RT-qPCR was performed on 11 pairs of GC and adjacent normal tissues, confirming a significant increase in DEPP1 mRNA expression in GC tissues (Fig. 1C). Consistently, western blotting revealed elevated protein levels of DEPP1 in GC tissues (Fig. 1D). Immunofluorescence staining further supported these observations, with DEPP1 exhibiting diffuse positivity in GC tissues while being barely detected in adjacent normal tissues (Fig. 1E). It is possible that DEPP1 is expressed in rare cell subsets or localized regions within adjacent tissues, which may not be adequately represented in immunofluorescence sections due to the sparsity of these cells. In contrast, western blotting analyzes protein from the entire tissue lysate, allowing for the detection of even minimal levels of DEPP1 expression. Furthermore, tissue fixation may impact antigen accessibility, while the denaturation of proteins during western blotting ensures optimal binding of antibodies. Collectively, these findings indicate significant upregulation of DEPP1 in GC, warranting further investigation.

The prognostic value of DEPP1 in GC. In the TCGA-STAD dataset, patients with GC exhibiting higher expression levels of DEPP1 experienced significantly shorter OS and DFS compared with those with lower DEPP1 expression (Fig. 2A and B). Consistently, individuals with GC who died or experienced tumor recurrence during follow-up showed substantially higher expression levels of DEPP1 (Fig. 2C and D). Moreover, significant differences in RMST were observed between low- and high-expression groups of DEPP1 at 36 and 60 months (Table I). Notably, the RMST difference increased from 4.116 months ($P=0.02$) at 36 months to 10.202 months ($P<0.01$) at 60 months. While EGFR and KRAS are recognized potent oncogenes and promising therapeutic targets in GC, DEPP1 (HR, 2.493; 95% CI, 1.326-4.688; $P<0.01$) was found to be a significant prognostic factor of GC, as demonstrated by univariate Cox regression analysis (Fig. 2E) (28). In addition to DEPP1, clinicopathologic characteristics including age (HR, 1.023; 95% CI, 1.006-1.039; $P<0.01$), histological grade (HR, 1.347; 95% CI, 1.006-1.804; $P<0.05$), and TNM stage (HR, 1.566; 95% CI, 1.275-1.924; $P<0.001$) were identified as prognostic factors of GC. Multivariate Cox regression analysis further confirmed DEPP1 as an independent prognostic factor (HR, 2.220; 95% CI, 1.145-4.303; $P<0.05$) in GC (Fig. 2F). ROC curves revealed that DEPP1 exhibited improved predictive capability for 5-year OS of patients with GC (AUC, 0.659) compared with traditional oncogenes such as EGFR (AUC, 0.568) and KRAS (AUC, 0.520) (Fig. 2G).

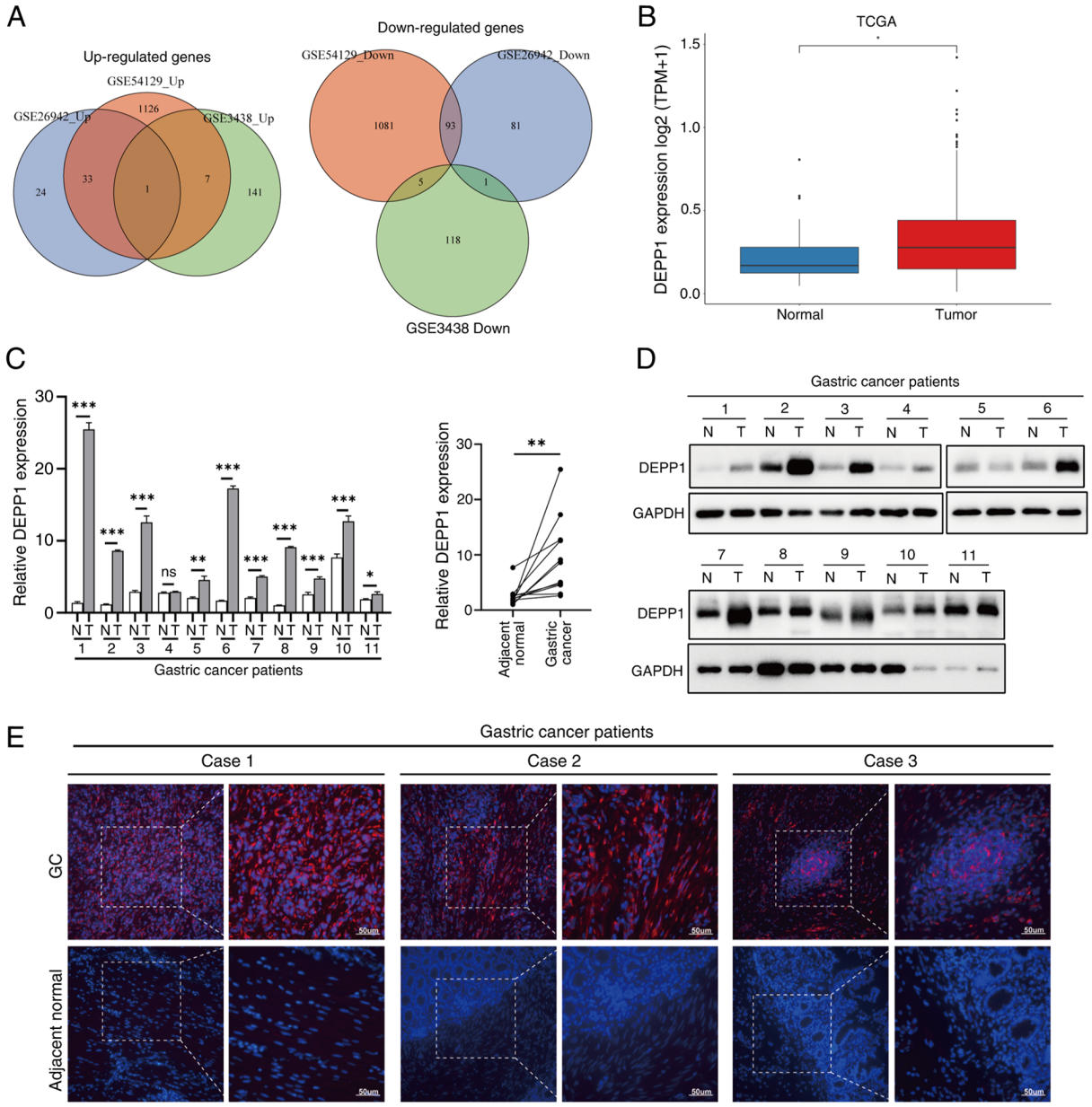

Figure 1. DEPP1 is aberrantly overexpressed in gastric cancer. (A) Venn diagrams illustrating the differentially expressed genes. (B) Expression levels of DEPP1 in GC and normal tissues in the TCGA-STAD cohort. Relative expression of DEPP1 in 11 pairs of GC and adjacent normal tissues measured by (C) reverse transcription-quantitative PCR and (D) western blotting. (E) Representative immunofluorescence images of DEPP1 in 11 pairs of GC and adjacent normal tissues. *P<0.05, **P<0.01 and ***P<0.001. DEPP1, decidual protein induced by progesterone; GC, gastric cancer; TCGA-STAD, The Cancer Genome Atlas Stomach Adenocarcinoma; N, normal; T, tumor; Ns, not significant.

Similarly, in the GSE84437 cohort, patients with lower DEPP1 expression levels exhibited longer OS compared with those with higher DEPP1 expression (Fig. 3A). Statistically significant RMST differences were observed at 12 months (0.627 months; 95% CI, 0.253-1.002 months; P<0.01), 36 months (3.433 months; 95% CI, 1.526-5.339 months; P<0.001), and 60 months (8.451 months; 95% CI, 4.705-12.198 months; P<0.001) (Table I). Univariate and multivariate Cox regression analyses confirmed DEPP1 as an independent prognostic indicator of GC (Fig. 3B and C). In the GSE15459 cohort, higher DEPP1 expression was associated with shorter OS in patients with GC (Fig. 3D). Significant RMST differences were observed at 36 months (4.286 months; 95% CI, 0.252-8.319 months; P<0.05) and 60 months (9.403 months; 95% CI, 1.944-16.861 months; P<0.05) (Table I). Univariate Cox regression analysis revealed DEPP1 (HR, 1.349; 95% CI, 1.047-1.739; P<0.05), KRAS (HR, 1.455; 95% CI, 1.087-1.946; P<0.05) and TNM stage (HR, 2.789; 95% CI, 2.140-3.635; P<0.001) as prognostic factors of GC (Fig. 3E). However, the independent prognostic effect of DEPP1 and KRAS was not evident except for TNM stage (Fig. 3F). To further clarify the prognostic role of DEPP1 in GC, an IHC assay was performed on 11 slides of normal gastric tissues and a tissue microarray containing 160 GC patient specimens. DEPP1 was diffusely overexpressed in GC tissues compared with normal gastric tissues, and patients with higher DEPP1 expression levels exhibited significantly shorter OS compared with those

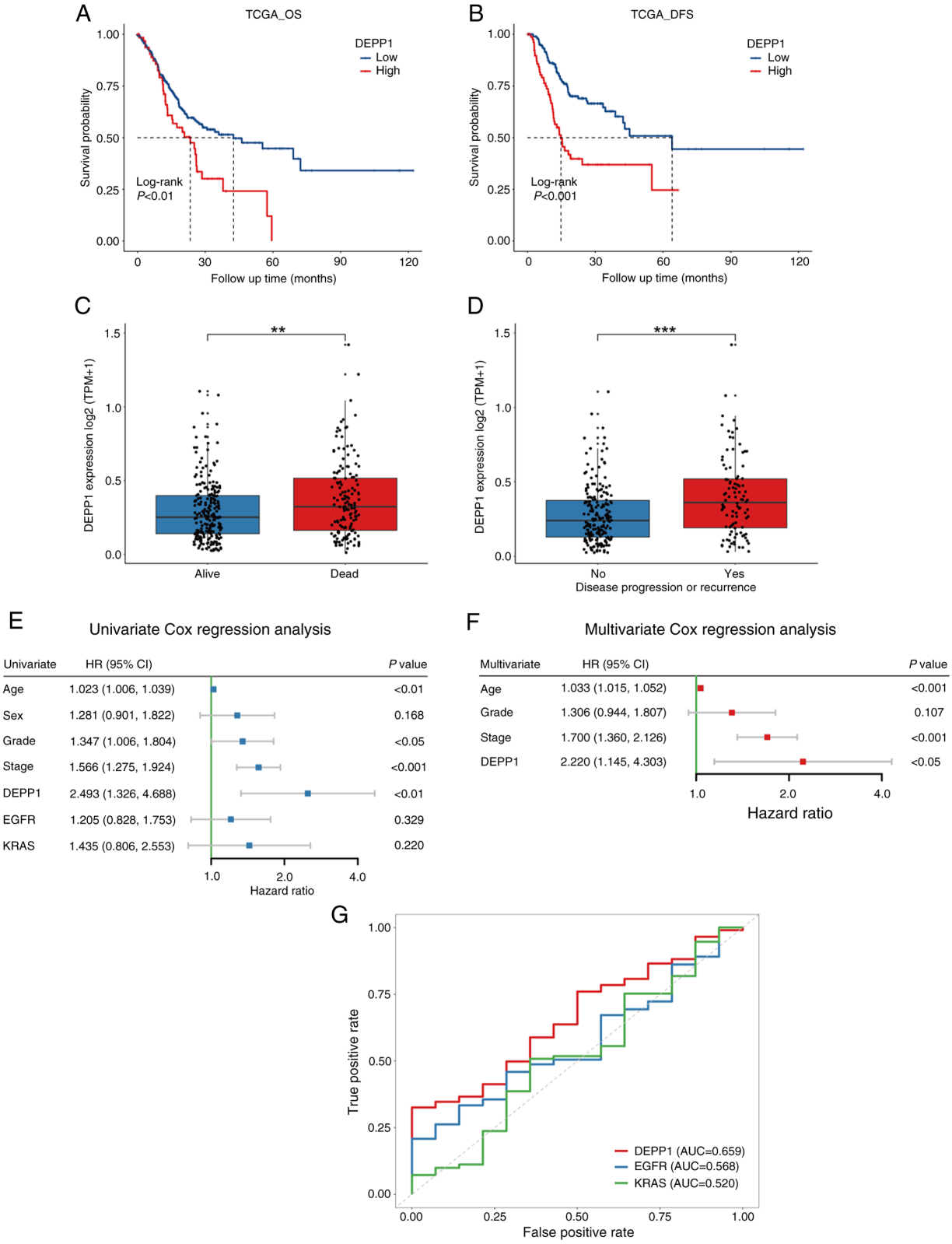

Figure 2. Prognostic value of DEPP1 is explored in the TCGA-STAD cohort. Kaplan-Meier survival analyses of DEPP1 in patients with GC on (A) overall survival and (B) disease-free survival. DEPP1 expression between patients with GC who are (C) alive or dead and (D) patients with or without disease progression or recurrence. (E) Univariate and (F) multivariate Cox regression analysis of DEPP1 and other clinicopathologic features. (G) Receiver operating characteristic curves of DEPP1 and conventional oncogenes EGFR and KRAS in predicting five-year overall survival of patients with GC. **P<0.01 and ***P<0.001. DEPP1, decidual protein induced by progesterone; TCGA-STAD, The Cancer Genome Atlas Stomach Adenocarcinoma; GC, gastric cancer; OS, overall survival; DFS, disease-free survival; HR, hazard ratio; CI, confidence interval.

with lower DEPP1 expression (Fig. 3G and H). The survival data and corresponding IHC scores of the Renji cohort were summarized in Table SVII. Collectively, DEPP1 emerges as a significant risk factor for patients with GC.

Table I. Restricted mean survival time differences between the low- and high-expression groups of DEPP1 at 12, 36 and 60 months.

Cohort	Time point (months)	RMST[a] Low expression (95% CI)	RMST[a] High expression (95% CI)	RMST difference[b]	P-value[c]
TCGA-STAD	12	10.812 (10.490, 11.135)	10.718 (10.048, 11.387)	0.095 (-0.648, 0.838)	0.803
cohort (n=375)	36	25.600 (23.994, 27.206)	21.484 (18.407, 24.561)	4.116 (0.645, 7.587)	0.020
	60	37.218 (33.940, 40.496)	27.016 (21.208, 32.825)	10.202 (3.532, 16.871)	0.003
GSE84437	12	11.708 (11.510, 11.905)	11.080 (10.762, 11.398)	0.627 (0.253, 1.002)	0.001
cohort (n=433)	36	31.971 (30.661, 33.280)	28.538 (27.152, 29.924)	3.433 (1.526, 5.339)	<0.001
	60	50.110 (47.414, 52.806)	41.659 (39.057, 44.260)	8.451 (4.705, 12.198)	<0.001
GSE15459	12	11.079 (10.663, 11.494)	10.574 (9.856, 11.291)	0.505 (-0.324, 1.334)	0.233
cohort (n=192)	36	26.433 (24.203, 28.662)	22.147 (18.786, 25.509)	4.286 (0.252, 8.319)	0.037
	60	38.778 (34.436, 43.119)	29.375 (23.310, 35.440)	9.403 (1.944, 16.861)	0.013

[a]RMST, restricted mean survival time; [b]RMST difference=$RMST_{Low\ expression}$-$RMST_{High\ expression}$; and [c]P<0.05 was considered statistically significant. CI, confidence interval; TCGA-STAD, The Cancer Genome Atlas Stomach Adenocarcinoma.

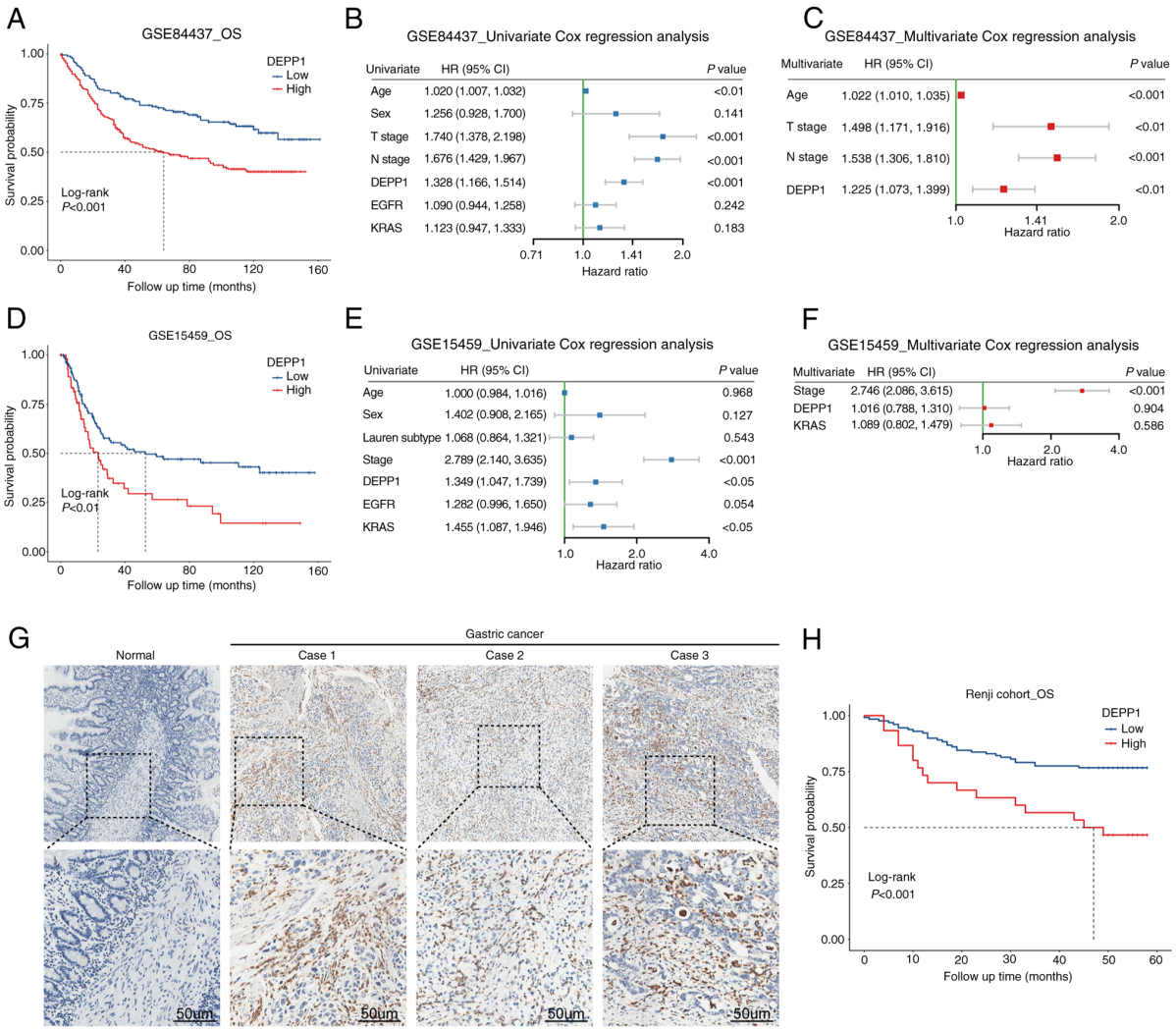

Figure 3. Prognostic value of DEPP1 is validated in GSE84437, GSE15459 and Renji cohorts. Kaplan-Meier survival analyses of DEPP1 on overall survival in (A) GSE84437 and (D) GSE15459 cohorts. (B) Univariate and (C) multivariate Cox regression analysis of DEPP1 and other clinicopathologic parameters in the GSE84437 cohort. (E) Univariate and (F) multivariate Cox regression analysis of DEPP1 and other clinicopathologic factors in the GSE15459 cohort. (G) Representative immunohistochemistry images of DEPP1 in gastric cancer and normal tissues. (H) Kaplan-Meier survival analysis of DEPP1 on overall survival in the Renji cohort. DEPP1, decidual protein induced by progesterone; OS, overall survival; DFS, disease-free survival; HR, hazard ratio; CI, confidence interval.

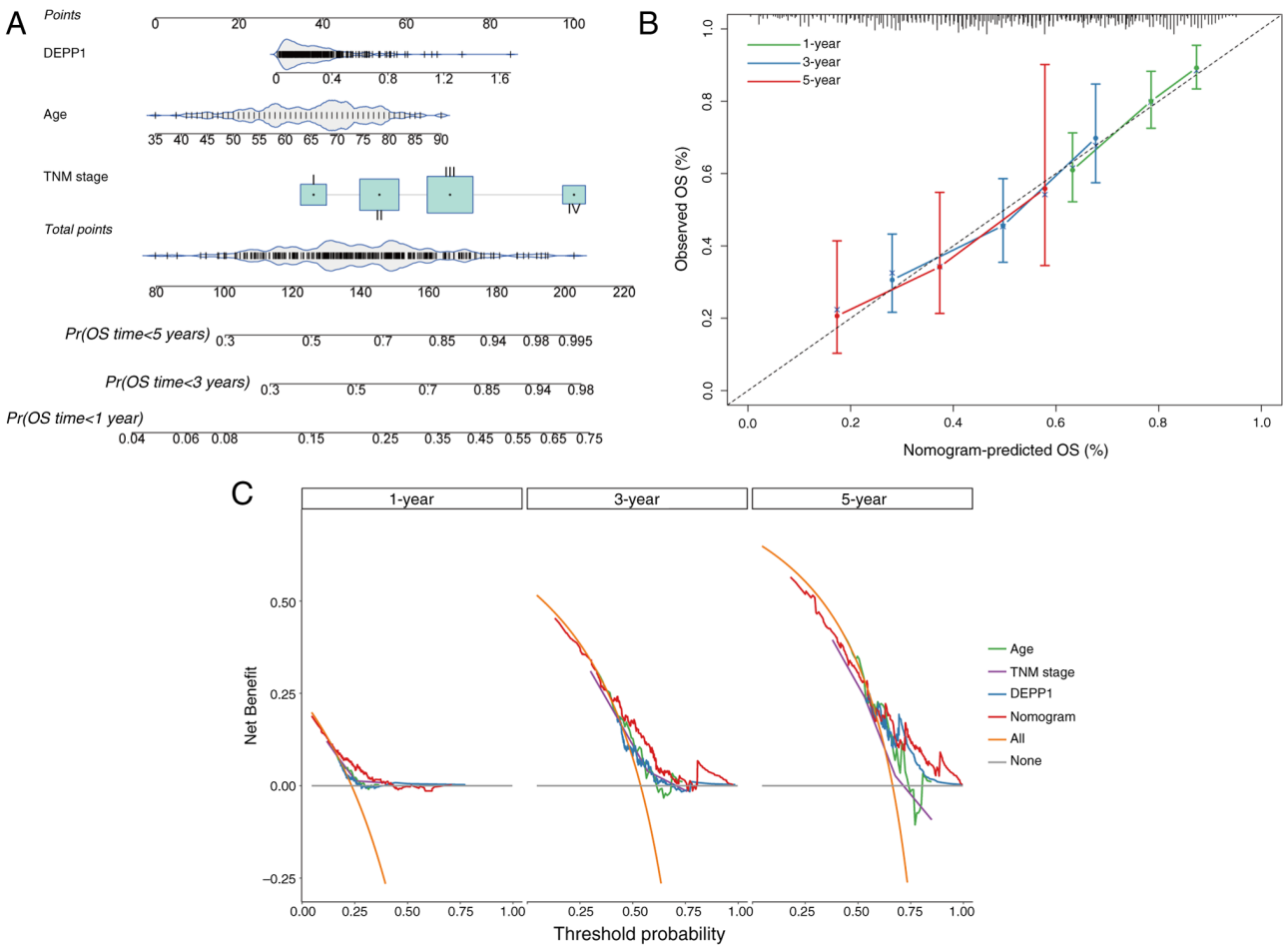

Figure 4. Establishment and evaluation of a prognostic nomogram for GC. (A) Construction of a nomogram integrating DEPP1, age and TNM stage to predict the 1-, 3- and 5-year overall survival of patients with GC. (B) Calibration curves to assess the predictive accuracy of the nomogram for survival outcomes. (C) Results of decision curve analysis comparing the nomogram's performance with that of individual predictors, including DEPP1, age and TNM stage. DEPP1, decidual protein induced by progesterone; GC, gastric cancer; TNM, tumor-node-metastasis; OS, overall survival; Pr, probability.

Construction and validation of a prognostic nomogram. In order to provide a quantitative tool for predicting the OS rate of patients with GC, a nomogram incorporating the expression level of DEPP1, patient age and TNM stage was developed. These factors were identified as independent prognostic indicators of GC based on the analysis of data from the TCGA-STAD cohort (Fig. 4A). The calibration curves demonstrated that the predicted 1-, 3- and 5-year OS rates from the nomogram closely matched the observed rates in patients with GC, indicating excellent predictive performance (Fig. 4B). Additionally, DCA showed that the composite nomogram provided greater clinical net benefit compared with DEPP1, age, or TNM stage alone at 1-, 3- and 5-year intervals (Fig. 4C). Overall, the nomogram enhances the predictive ability of the TNM staging system for OS rates of patients with GC.

Association between DEPP1 and clinicopathologic factors of patients with GC. Lauren's classification categorizes GC into intestinal, diffuse and mixed phenotypes, with the diffuse phenotype typically associated with therapy resistance and poor prognosis (29,30). The present analysis revealed that patients with GC with the diffuse phenotype exhibited significantly higher expression levels of DEPP1 compared with those with intestinal or mixed phenotypes in the GSE15459 cohort (Fig. 5A). Logistic regression analysis identified DEPP1 as a significant risk factor for the diffuse phenotype (Table II; diffuse vs. intestinal phenotype; OR, 2.288; 95%CI, 1.504-3.480; P<0.001). Additionally, DEPP1 was significantly associated with histological grade in the TCGA-STAD cohort (Table SVIII). Stratified analysis revealed that higher DEPP1 expression was associated with shorter OS across all histological subtypes of GC, indicating consistent predictive value across different subtypes (Fig. 5B).

Furthermore, significantly higher DEPP1 expression was observed in advanced-stage patients with GC compared with those at stage I (Fig. 5C). DEPP1 was identified as a significant risk factor for advanced TNM stages (Table II; stage II vs. stage I; OR, 15.467; 95% CI, 2.239-106.843; P=0.005; stage III vs. stage I; OR, 8.672; 95% CI, 1.291-58.226; P<0.05). Patients with higher DEPP1 expression levels across all stages had substantially shorter OS (Fig. 5D). Similarly, concerning local infiltration depth, tumors with deeper infiltration exhibited significantly higher DEPP1 expression levels (Fig. 5E), and higher DEPP1 expression associated with deeper infiltration (Fig. 5F and G). Logistic regression analysis indicated DEPP1 as a significant risk factor for advanced T stages (Table II; T4 vs. T1; OR, 2.755; 95% CI, 1.419-5.346; P<0.01). Stratified analysis based on infiltration depth revealed that higher DEPP1

Table II. Correlation between DEPP1 expression and clinical features using logistic regression.

Cohorts	Clinical features		OR	95% CI	P-value[a]
TCGA-STAD cohort (n=375)	TNM stage	II vs. I	15.467	2.239-106.843	0.005
		III vs. I	8.672	1.291-58.226	0.026
		IV vs. I	8.94	0.938-85.220	0.057
GSE84437 cohort (n=433)	T stage	T2 vs. T1	1.434	0.697-2.949	0.328
		T3 vs. T1	1.644	0.836-3.235	0.150
		T4 vs. T1	2.755	1.419-5.346	0.003
GSE15459 cohort (n=192)	Lauren phenotype	Diffuse vs. intestinal	2.288	1.504-3.480	<0.001
		Mixed vs. intestinal	1.289	0.704-2.360	0.412

[a]P<0.05 was considered statistically significant. DEPP1, decidual protein induced by progesterone; OR, odds ratio; 95% CI, 95% confidence interval.

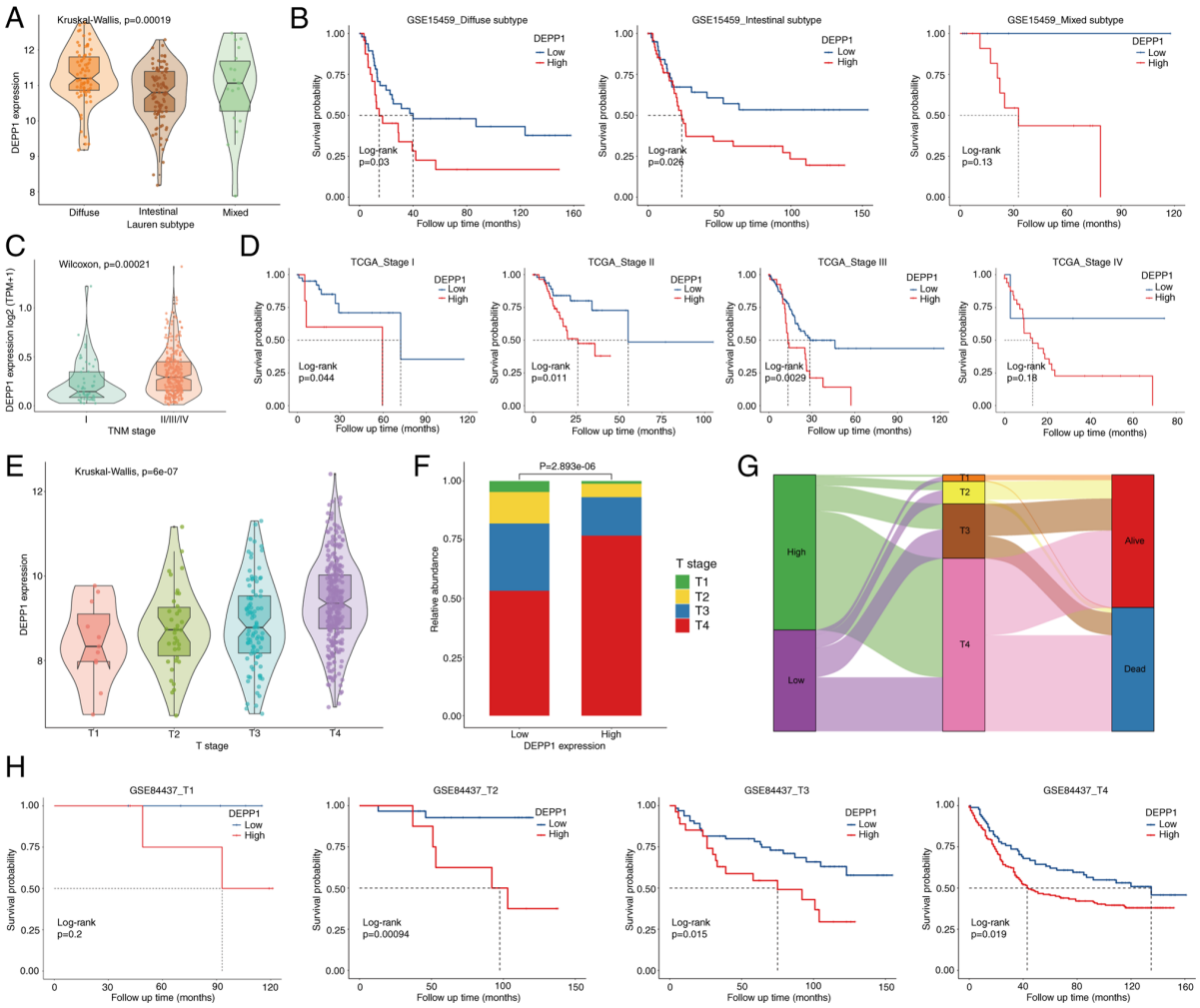

Figure 5. Relationship between DEPP1 expression and clinicopathologic factors in patients with GC. (A) DEPP1 expression levels across different Lauren phenotypes. (B) Kaplan-Meier survival analyses of DEPP1 in diffuse, intestinal and mixed subtypes of the GSE15459 cohort. (C) DEPP1 expression levels in stage I and advanced stages of GC. (D) Kaplan-Meier survival analyses of DEPP1 in stage I, II, III and IV of the TCGA-STAD cohort. (E) DEPP1 expression levels across distinct T stages. (F) The histogram displaying the distribution of T stages between the low- and high-expression groups of DEPP1. (G) The alluvial diagram depicting the association between DEPP1 expression, T stages and overall survival status. (H) Kaplan-Meier survival analyses of DEPP1 in T1, T2, T3 and T4 stages of the GSE84437 cohort. DEPP1, decidual protein induced by progesterone; GC, gastric cancer; TCGA-STAD, The Cancer Genome Atlas Stomach Adenocarcinoma.

expression was associated with shorter OS across all T stages (Fig. 5H). Overall, DEPP1 serves as a potent risk factor for TNM and T stages and an effective prognostic biomarker across distinct stages.

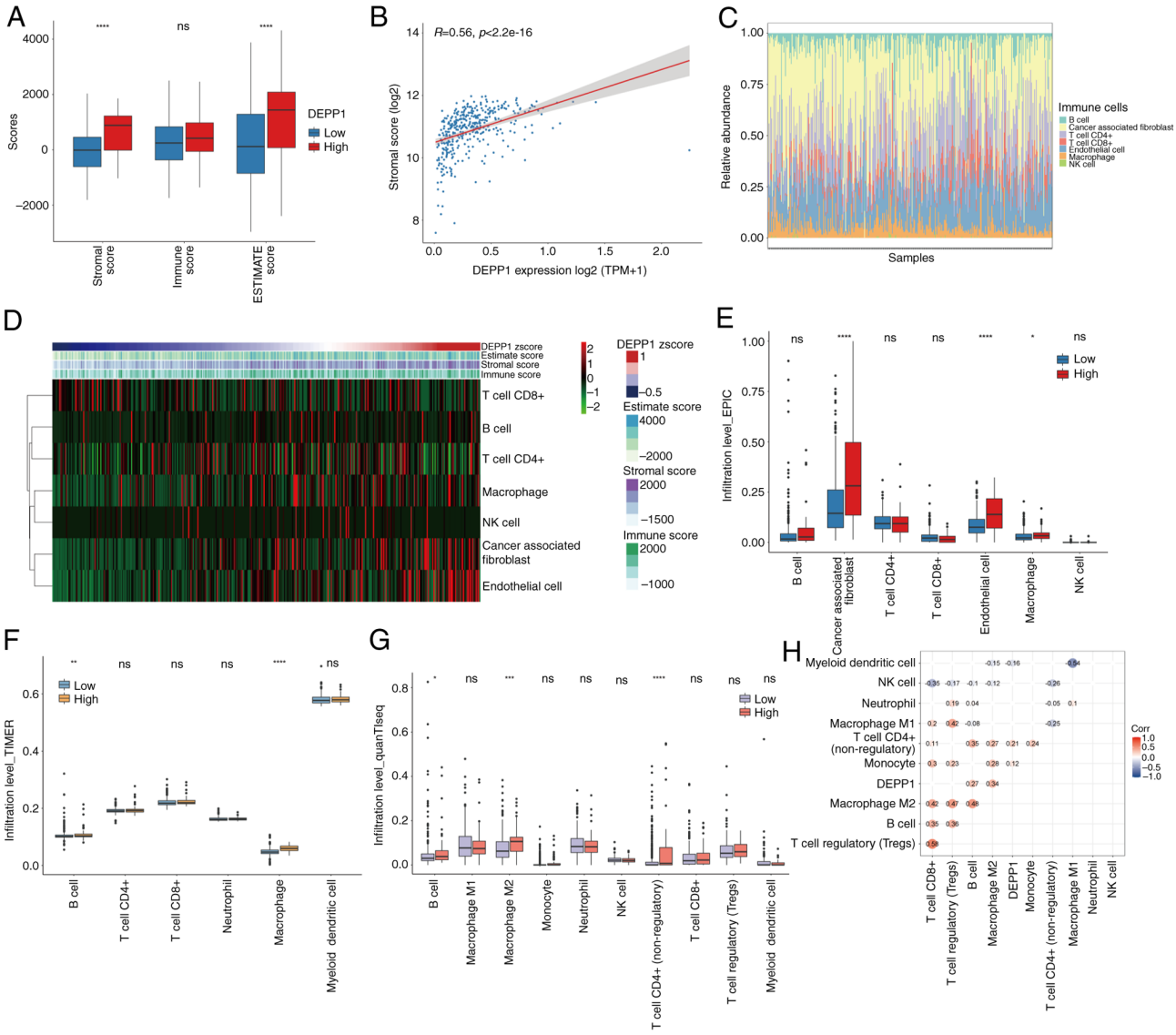

Figure 6. DEPP1 correlates with a stroma-rich and immunosuppressive microenvironment of GC. (A) The stromal, immune, and estimate scores in the low- and high-expression groups of DEPP1. (B) The correlation between DEPP1 expression and stromal score. (C) The distribution of various immune and stromal cells in the GC microenvironment estimated by the EPIC algorithm. (D) The heatmap showing the correlation between DEPP1 expression and immune and stromal cell populations. The infiltration levels of distinct immune and stromal cells in the low- and high-expression groups of DEPP1, as assessed by (E) EPIC, (F) TIMER and (G) quanTIseq methods, respectively. (H) A correlation heatmap illustrating the relationships between DEPP1 expression and various immune and stromal cells based on the results of the quanTIseq algorithm. *P<0.05, **P<0.01, ***P<0.001 and ****P<0.0001. DEPP1, decidual protein induced by progesterone; GC, gastric cancer; NK, natural killer; ns, not significant.

Association between DEPP1 and stroma-rich and immunosuppressive microenvironment of GC. The TME has emerged as a hallmark of cancer, garnering increasing attention in recent years for its significant role in tumorigenesis (31). In the present study, the correlation between DEPP1 expression and the TME in GC was investigated. It was observed that GC with higher DEPP1 expression exhibited significantly elevated stromal scores, indicating increased infiltration of stromal cells within tumor tissues (Fig. 6A; Table SIX). Moreover, a positive correlation was identified between DEPP1 expression and stromal score, suggesting a potential role of DEPP1 in shaping the stromal component of the GC microenvironment (Fig. 6B).

The landscape of the GC TME, as assessed by the EPIC algorithm, revealed an increase in the infiltration levels of CAFs and ECs with higher DEPP1 expression (Fig. 6C and D). Concurrently, macrophage infiltration also exhibited a slight positive correlation with DEPP1 expression. Additionally, tumors with higher DEPP1 expression showed significantly elevated levels of CAFs, ECs and macrophages compared with those with lower DEPP1 expression (Fig. 6E).

Further analysis using the TIMER algorithm demonstrated increased infiltration rates of macrophages and B cells in the high-expression group of DEPP1 (Fig. 6F). The quanTIseq method revealed higher infiltration of M2 macrophages, but not M1 macrophages, in GC tumors expressing higher levels of DEPP1 (Fig. 6G). The correlation heatmap indicated a significant positive association between DEPP1 expression and various immune and stromal cell populations, particularly M2 macrophages (Fig. 6H). Collectively, these findings suggest that DEPP1 plays a pivotal role in shaping the GC TME by promoting the recruitment of CAFs and

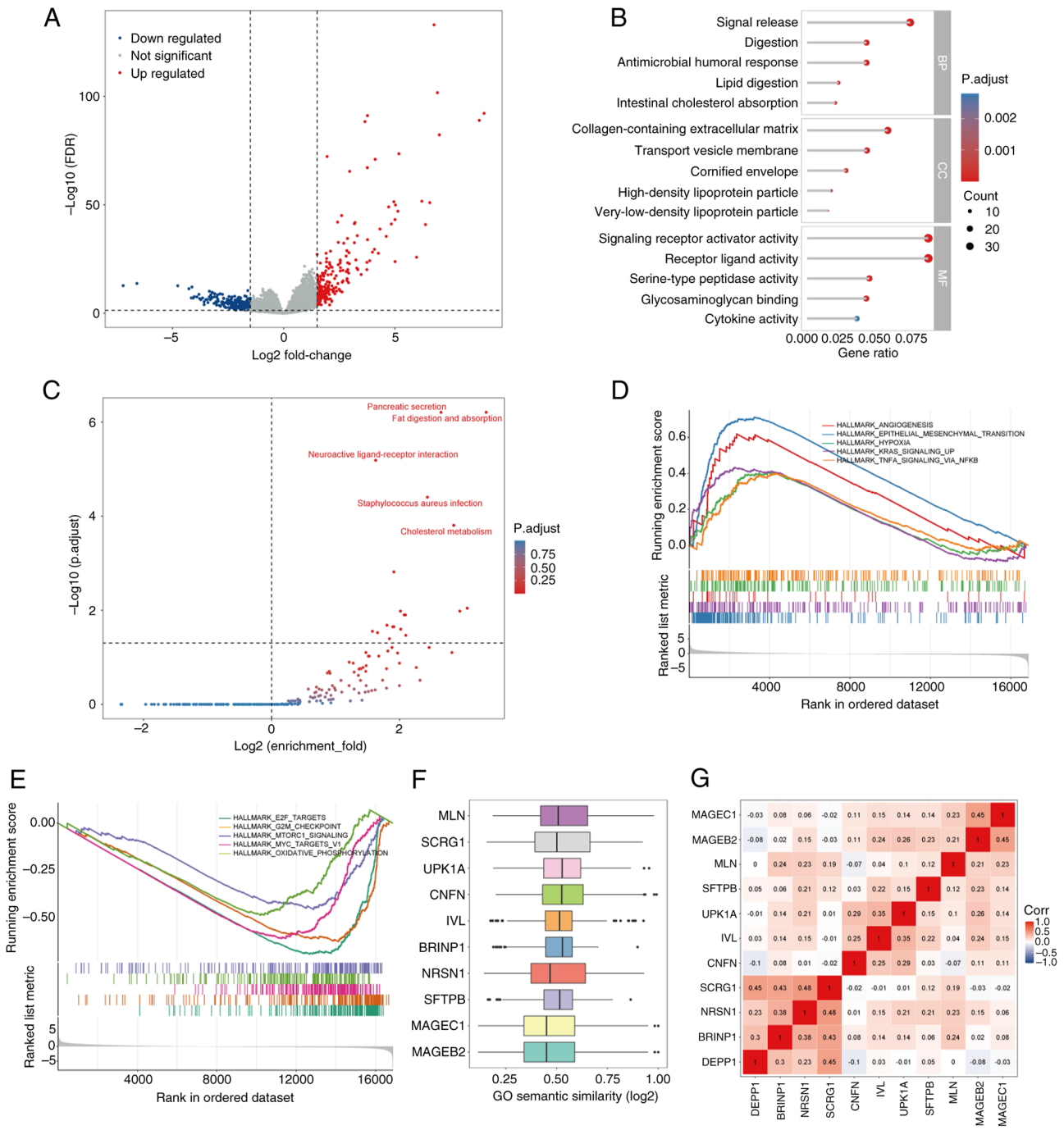

Figure 7. Potential regulatory mechanisms underlying DEPP1. (A) The volcano plot depicting the differentially expressed genes between the low- and high-expression groups of DEPP1. (B) Gene Ontology and (C) Kyoto Encyclopedia of Genes and Genome enrichment analyses of the differentially expressed genes. Gene Set Enrichment Analysis demonstrates the hallmark pathways enriched in the (D) high- and (E) low-expression groups of DEPP1. (F) The box plot of the downstream hub genes of DEPP1. (G) The correlation heatmap displays the relationships among the hub genes. DEPP1, decidual protein induced by progesterone.

ECs and inducing the polarization of TAMs towards an immunosuppressive M2 phenotype, thereby contributing to the establishment of a stromal-rich and immunosuppressive microenvironment.

Exploration of the potential regulatory mechanisms of DEPP1. Given the association of high DEPP1 expression with poor prognosis, advanced TNM stage, and a stroma-rich, immunosuppressive TME in GC, the authors sought to elucidate the underlying regulatory mechanisms of DEPP1. Differential expression analysis identified 216 upregulated and 251 downregulated genes in the high-expression group of DEPP1 (Fig. 7A; Table SX). GO enrichment analysis revealed enrichment in signal release, signaling receptor activator activity, receptor-ligand activity, lipid digestion, intestinal cholesterol absorption, and the collagen-containing extracellular matrix (Fig. 7B; Table SXI). Similarly, KEGG analysis highlighted pathways such as pancreatic secretion, fat digestion and absorption, and neuroactive ligand-receptor interaction (Fig. 7C; Table SXII).

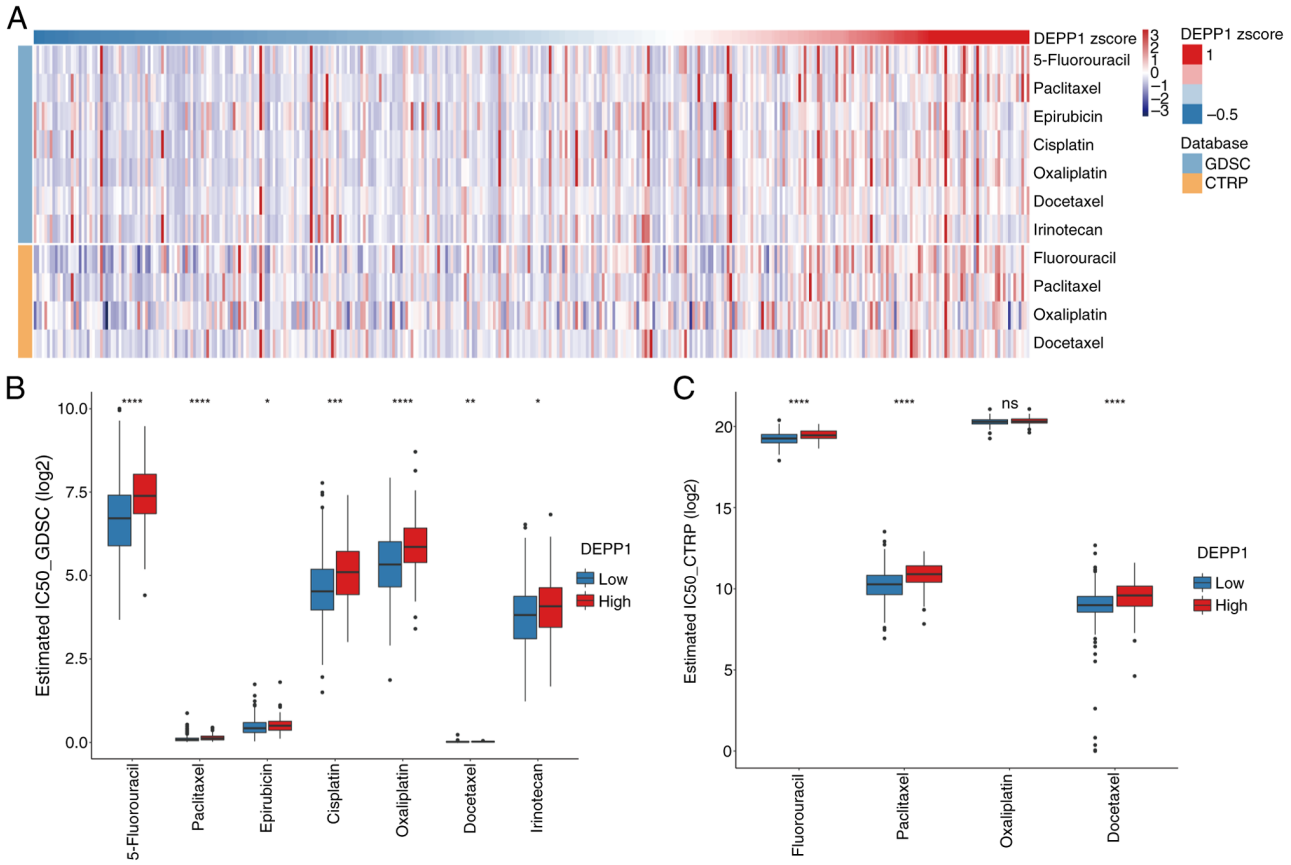

Figure 8. High DEPP1 expression predicts poor chemotherapy sensitivity in patients with GC. (A) The association between DEPP1 expression levels and the IC_{50} of selective chemotherapy drugs as shown by the heatmap. The estimated IC_{50} of chemotherapy drugs in the low- and high-expression groups of DEPP1, as analyzed using data from the (B) GDSC and (C) CTRP datasets, respectively. *P<0.05, **P<0.01, ***P<0.001 and ****P<0.0001. DEPP1, decidual protein induced by progesterone; GC, gastric cancer; IC_{50}, half-maximal inhibitory concentration; GDSC, Genomics of Drug Sensitivity in Cancer; CTRP, Cancer Therapeutics Response Portal; ns, not significant.

GSEA further uncovered enrichment of hallmark pathways, such as angiogenesis, epithelial-mesenchymal transition (EMT), hypoxia, KRAS signaling, and TNFα signaling via NFκB in the high-expression group of DEPP1 (Fig. 7D; Table SXIII). Conversely, pathways including E2F targets, G2M checkpoint, MTORC1 signaling, MYC targets and oxidative phosphorylation were enriched in the low-expression group (Fig. 7E; Table SXIII).

Subsequently, the Friends analysis identified downstream hub genes of DEPP1, including MLN, SCRG1, UPK1A, CNFN, IVL, BRINP1, NRSN1, SFTPB, MAGEC1 and MAGEB2, based on semantic similarity of GO terms (Fig. 7F; Table SXIV). These hub genes exhibited significant correlations, suggesting potential coordinated regulatory roles with DEPP1 in GC (Fig. 7G).

The prediction of chemotherapy sensitivity. Chemotherapy remains a cornerstone in the treatment of GC, particularly for patients with local non-resectable, recurrent, or metastatic disease (32). To assess the predictive effect of DEPP1 on chemotherapy sensitivity in GC, the IC_{50} of select chemotherapy agents was estimated by using data from GDSC and CTRP datasets (Tables SXV and SXVI). Notably, the IC_{50} of these drugs increased with DEPP1 expression, indicating a potential association between high DEPP1 expression and decreased chemotherapy sensitivity (Fig. 8A). Consistently, patients with GC with higher DEPP1 expression exhibited significantly higher IC_{50} values for these drugs compared with those with lower DEPP1 expression, corroborating that increased DEPP1 expression may predict poor chemotherapy sensitivity in patients with GC (Fig. 8B and C).

DEPP1 promotes oxaliplatin resistance in GC cells in vitro. Given the association between elevated *DEPP1* expression and increased IC_{50} values for chemotherapy agents, the authors investigated whether these agents could regulate DEPP1 expression. Remarkably, treatment with oxaliplatin and 5-FU upregulated DEPP1 expression in MKN45 and HGC27 cells (Fig. 9A and B). This finding prompted the hypothesis that DEPP1 may regulate chemotherapy resistance in GC. Therefore, the authors focused on oxaliplatin for further analysis.

Using lentiviral vectors, the authors successfully overexpressed DEPP1 in MKN45 and HGC27 cells, as verified by RT-qPCR and western blotting (Fig. 9C and D). It was observed that ectopic DEPP1 expression had little effect on MKN45 cell proliferation (Fig. 9E) and a slightly promoting effect on HGC27 (Fig. S2A). Of note, DEPP1 overexpression significantly enhanced the proliferation of MKN45 cells following a 24-h treatment with oxaliplatin (Fig. 9F), and a similar trend, though not statistically significant, was observed in HGC27 cells (Fig. S2B).

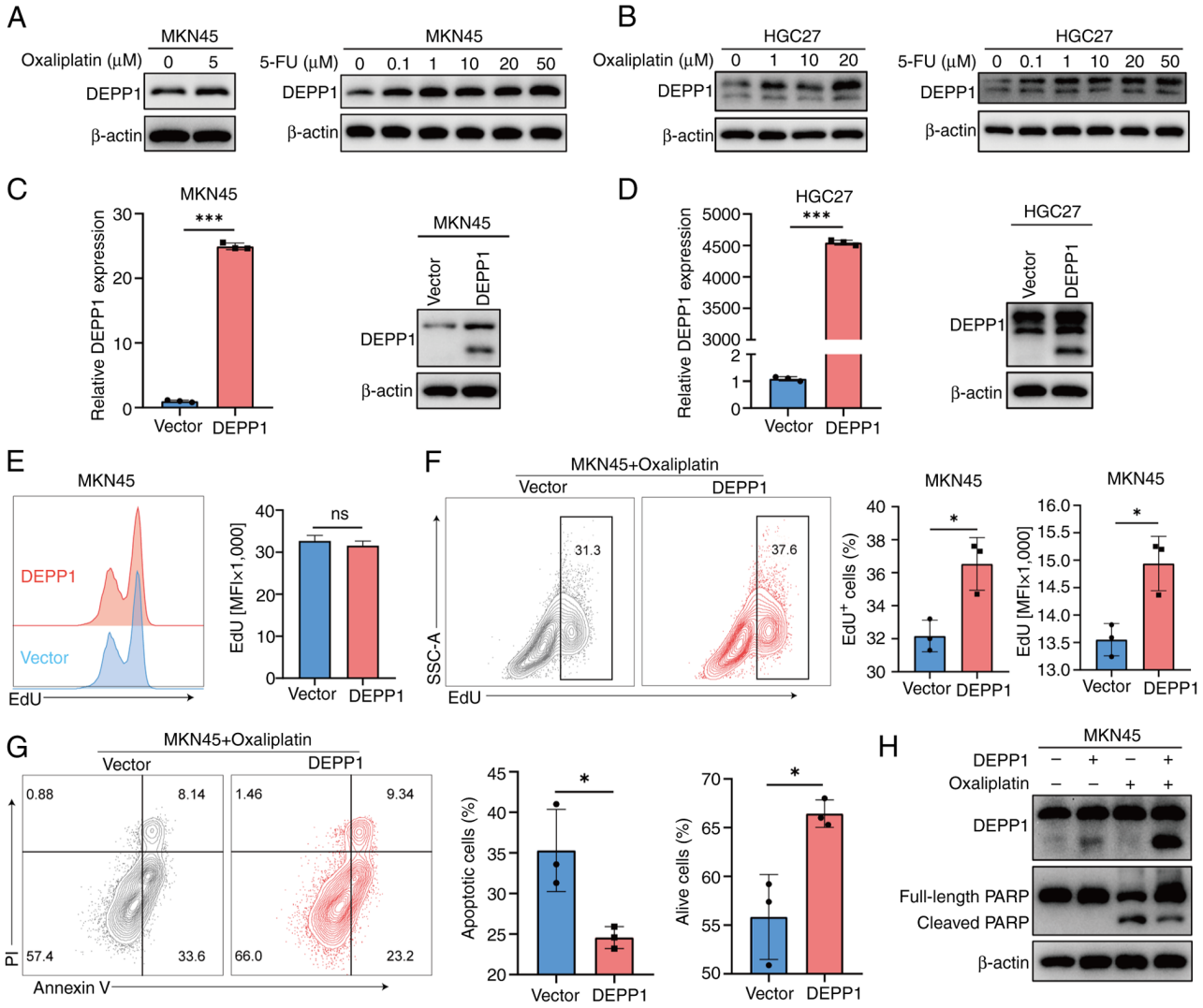

Figure 9. DEPP1 enhances oxaliplatin resistance in gastric cancer cells *in vitro*. Effects of oxaliplatin and fluorouracil supplementation on DEPP1 protein levels in (A) MKN45 and (B) HGC27 cells, respectively. Validation of DEPP1 overexpression in (C) MKN45 and (D) HGC27 cells. (E) Impact of DEPP1 overexpression on MKN45 cell proliferation, assessed using EdU flow cytometry. (F) Influence of DEPP1 overexpression on MKN45 proliferation following a 24-h treatment with 10 μM oxaliplatin. (G) Effects of ectopic DEPP1 expression on oxaliplatin-induced apoptosis (20 μM) in MKN45 cells, as measured by Annexin V/PI flow cytometry. (H) Analysis of full-length and cleaved PARP protein levels following forced DEPP1 expression in (H) MKN45 and (J) HGC27 cells. *P<0.05 and ***P<0.001 DEPP1, decidual protein induced by progesterone. ns, not significant.

It was further examined whether DEPP1 modulates oxaliplatin-induced apoptosis. Flow cytometry results indicated that increased DEPP1 expression reduced apoptosis and enhanced cell survival under oxaliplatin treatment (Figs. 9G and S2C). Additionally, DEPP1 overexpression led to a marked decrease in cleaved PARP protein levels, in MKN45 cells (Fig. 9H), whereas this effect was less pronounced in HGC27 cells (Fig. S2D). It was also discovered that ectopic DEPP1 expression attenuated the migratory abilities of GC cells (Fig. S2E and F). These findings collectively demonstrated that DEPP1 may enhance oxaliplatin resistance in GC cells *in vitro*.

DEPP1 promotes oxaliplatin resistance in GC cells in vivo. Building on the *in vitro* observations, the impact of DEPP1 on oxaliplatin resistance was assessed *in vivo*. Control and DEPP1-overexpressing MKN45 cells were subcutaneously injected into the right flanks of nude mice, followed by intraperitoneal administration of oxaliplatin or 5% glucose saline at a dosage of 5 mg/kg (Fig. 10A). All mice survived during the treatment and were euthanized via cervical dislocation 12 days post-treatment. Consistent with *in vitro* results, ectopic DEPP1 expression did not affect MKN45 tumor growth *in vivo* but maintained tumor growth in the presence of oxaliplatin (Fig. 10B-D). An induction of DEPP1 expression was observed in GC tissues following oxaliplatin treatment (Fig. 10D). Importantly, the pronounced apoptosis induced by oxaliplatin was significantly attenuated by DEPP1 overexpression, thereby confirming DEPP1's role in promoting oxaliplatin resistance in GC (Fig. 10D).

Discussion

GC ranks as the fifth most diagnosed malignancy and the fourth leading cause of cancer-related deaths globally, posing a significant threat to public health (2). Common symptoms of

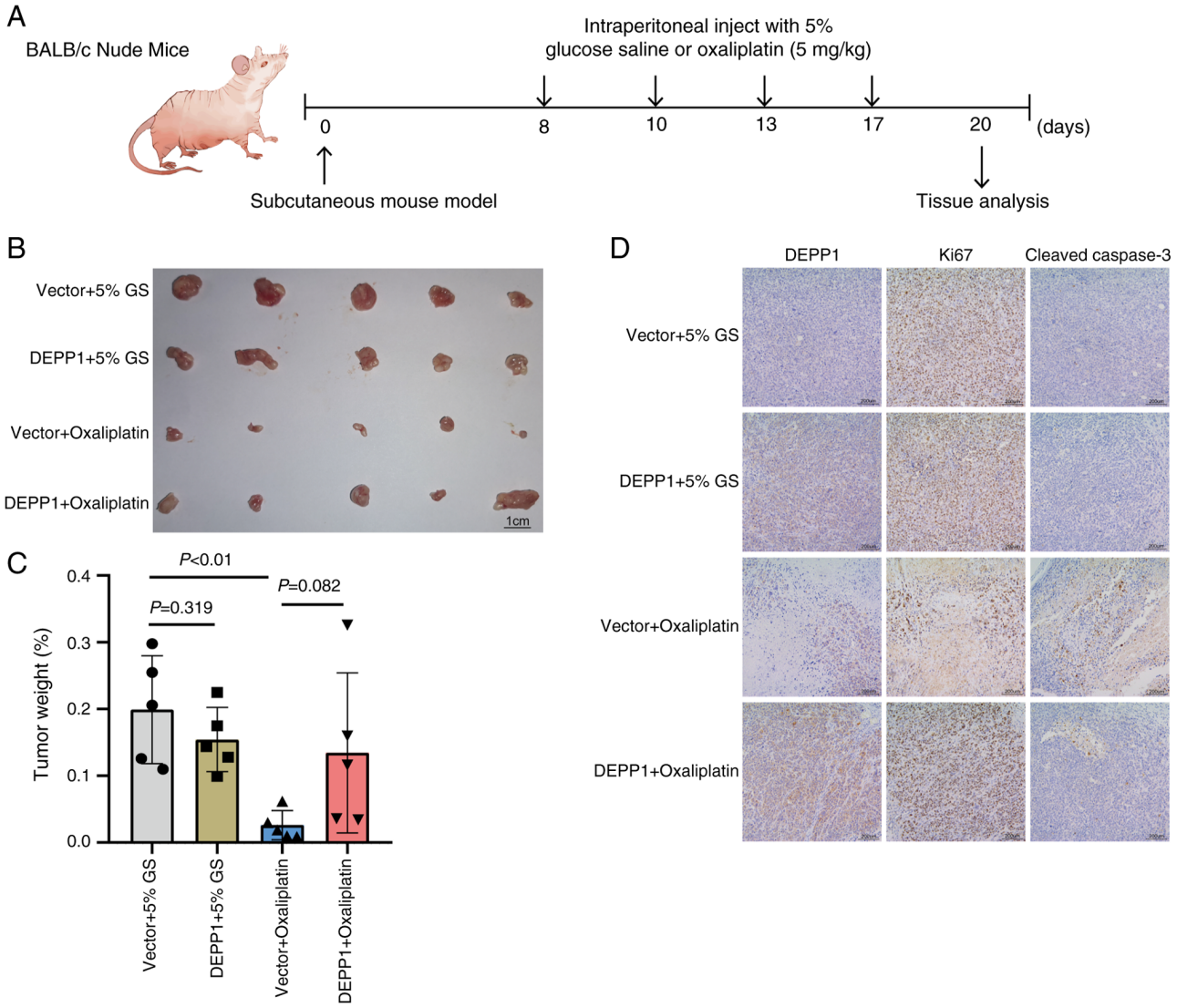

Figure 10. DEPP1 enhances oxaliplatin resistance in gastric cancer cells *in vivo*. (A) Schematic representation of the subcutaneous mouse model receiving either 5% GS or 5 mg/kg oxaliplatin intraperitoneally. (B) Images and (C) weights of control and DEPP1-overexpressing tumors treated with or without oxaliplatin. (D) Representative immunohistochemistry images of DEPP1, Ki67, and cleaved caspase 3 in subcutaneous tumor tissues. DEPP1, decidual protein induced by progesterone; GS, glucose saline.

GC include indigestion, anorexia, weight loss and abdominal pain. However, the disease is often diagnosed at an advanced stage, rendering it incurable and resulting in poor prognosis (32). Advanced GC frequently presents with peritoneal or liver metastasis, further exacerbating prognosis (30,33). The present study revealed a significant overexpression of DEPP1 in GC tissues compared with normal gastric tissues at both RNA and protein levels, suggesting its potential as a biomarker for GC. Given DEPP1's heterogenous roles in several cancers, the authors aimed to investigate its impact on GC, an aspect not previously addressed.

The American Joint Committee on Cancer TNM staging system serves as the primary tool for evaluating GC patient prognosis. However, its predictive efficiency varies, as patients in the same stage exhibit significantly distinct survival outcomes (34). Therefore, there is a pressing need to identify novel prognostic biomarkers for GC to complement the TNM staging system. The present study identified high DEPP1 expression as predicting poor OS in patients with GC across multiple cohorts, which was further validated by IHC testing in our cohort. Additionally, DEPP1, along with TNM stage, emerged as an independent risk factor for GC in TCGA-STAD and GSE84437 cohorts. Notably, DEPP1 outperformed classical oncogenes such as EGFR and KRAS in predicting prognosis, highlighting its potential as a promising prognostic biomarker for GC. Moreover, DEPP1 expression correlated significantly with TNM and T stages, underscoring its critical role in GC progression. To enhance the predictive accuracy of the TNM staging system, a nomogram incorporating DEPP1 expression, age, and TNM stage was developed, demonstrating superior predictive ability over the TNM staging system alone.

The TME, comprising various stromal and immune cells, exerts a crucial influence on tumor progression, including GC (35). Intriguingly, a positive correlation was observed between elevated DEPP1 expression and stromal score in the GC TME, suggesting increased stromal cell infiltration. Notably, the diffuse type of GC, characterized by

excessive stroma deposition and aggressive phenotypes, exhibited significantly higher DEPP1 expression compared with other phenotypes (29,30). CAFs constitute a pivotal component of the TME, actively participating in cancer progression through ECM generation and remodeling, as well as secretion of diverse molecules, exosomes, and metabolites (36). ECs also hold significant importance within the TME, contributing to immunosuppression and facilitating remote dissemination of cancer cells (37,38). In the present study, DEPP1 expression displayed a positive correlation with infiltration rates of both CAFs and ECs. Furthermore, significant enrichment of downstream genes associated with *DEPP1* was observed in the collagen-containing extracellular matrix, indicating a potential regulatory role for DEPP1 in the stromal component of the TME.

TAMs exhibit diverse phenotypes in the TME, with M2 macrophages promoting an immunosuppressive microenvironment conducive to tumor progression (39). The findings of the present study revealed a positive correlation between DEPP1 expression and M2 macrophage infiltration in the GC TME, suggesting DEPP1 as a potential biomarker for an immunosuppressive microenvironment. Angiogenesis and hypoxia are established hallmarks of TME of most solid tumors (31,40). The stromal and immune cells in the TME can secret a wide range of cytokines and chemokines, such as TGFβ, IL-6, and CCL18, to induce the EMT of tumor cells (41). The present study demonstrated that pathways related to angiogenesis, hypoxia, and EMT were enriched in the subgroup with higher DEPP1 expression, implicating potential mechanisms underlying the stroma-rich and immunosuppressive TME associated with DEPP1.

Despite advancements in immunotherapy and targeted therapy, chemotherapy remains a cornerstone in GC treatment, particularly for unresectable or metastatic disease. Chemotherapy significantly improves the median quality-adjusted survival time from 2 to 6 months for patients with GC with surgically non-curable diseases (42). Nevertheless, the majority of patients eventually develop chemotherapy resistance, leading to rapid disease progression and mortality (43). The present study demonstrated that high DEPP1 expression correlated with poor chemotherapy sensitivity. *In vitro* and *in vivo* experiments confirmed that oxaliplatin treatment induces DEPP1 expression, which in turn protects GC cells from apoptosis. Interestingly, overexpression of DEPP1 was also observed to suppress the migration of GC cells. Previous reports suggest that DEPP1 is upregulated in challenging conditions, such as hypoxia, and can activate autophagy (44,45). Emerging evidence indicates that autophagy may inhibit EMT and Rho GTPase activity, thereby reducing tumor metastasis (46). These findings suggest that DEPP1 functions as a critical regulator, promoting oxaliplatin resistance while simultaneously suppressing the migratory ability of GC cells in the nutrient-deficient TME.

There are several limitations to the present study. First, the expression status of DEPP1 in oxaliplatin-resistant human GC specimens has yet to be explored. Second, in the subcutaneous mouse model, while DEPP1 overexpression appeared to maintain tumor growth following oxaliplatin administration, this effect did not reach statistical significance due to substantial heterogeneity and small sample sizes. Additionally, the apoptosis-protective effect of *DEPP1* exhibited variability across different GC cell lines, possibly attributable to intrinsic differences in genetic backgrounds and apoptotic pathway dependencies. This variability emphasizes the need for further validation in primary GC models, such as organoids. Third, the molecular mechanisms underlying DEPP1-mediated oxaliplatin resistance warrant further investigation.

In conclusion, the authors highlight DEPP1 as an independent prognostic biomarker with the potential to enhance the predictive accuracy of the TNM staging system. Furthermore, its association with a stroma-rich and immunosuppressive microenvironment is elucidated. Most importantly, DEPP1's role in promoting oxaliplatin resistance is underscored, positioning it as a promising therapeutic target for overcoming chemoresistance in GC patients.

Acknowledgements

Not applicable.

Funding

The present study was supported by the National Natural Science Foundation of China (grant no. 82072669; and 81702303) and CSCO-Zaiding Cancer Research Fund (grant no. Y-zai2021/ms-0228).

Availability of data and materials

The data generated in the present study are included in the figures and tables of this article.

Authors' contributions

XQ, TP, and TK conceived the study and drafted the manuscript. YS, YZ, HG, and BN collected the data. XX, CZ, and ZZ analyzed and interpreted the data. HC and LT revised the manuscript and supervised the study. HC and LT confirm the authenticity of all the raw data. All authors read and approved the final version of the manuscript.

Ethics approval and consent to participate

The present study adhered to the principles outlined in The Declaration of Helsinki and obtained approval from the Ethics Committee of Renji Hospital, Shanghai Jiao Tong University School of Medicine (approval no. KY2021-252-B; Shanghai, China). Written informed consent was obtained from all participants included in the study, encompassing a statement on the collection and utilization of clinical samples for scientific research purposes.

Patient consent for publication

Not applicable.

Competing interests

The authors declare that they have no competing interests.

References

1. Thrift AP, Wenker TN and El-Serag HB: Global burden of gastric cancer: Epidemiological trends, risk factors, screening and prevention. Nat Rev Clin Oncol 20: 338-349, 2023.
2. Sung H, Ferlay J, Siegel RL, Laversanne M, Soerjomataram I, Jemal A and Bray F: Global cancer statistics 2020: GLOBOCAN estimates of incidence and mortality worldwide for 36 cancers in 185 countries. CA Cancer J Clin 71: 209-249, 2021.
3. de Visser KE and Joyce JA: The evolving tumor microenvironment: From cancer initiation to metastatic outgrowth. Cancer Cell 41: 374-403, 2023.
4. Wang R, Song S, Qin J, Yoshimura K, Peng F, Chu Y, Li Y, Fan Y, Jin J, Dang M, *et al*: Evolution of immune and stromal cell states and ecotypes during gastric adenocarcinoma progression. Cancer Cell 41: 1407-1426.e9, 2023.
5. Guan WL, He Y and Xu RH: Gastric cancer treatment: Recent progress and future perspectives. J Hematol Oncol 16: 57, 2023.
6. Watanabe H, Nonoguchi K, Sakurai T, Masuda T, Itoh K and Fujita J: A novel protein Depp, which is induced by progesterone in human endometrial stromal cells activates Elk-1 transcription factor. Mol Hum Reprod 11: 471-476, 2005.
7. Salcher S, Hagenbuchner J, Geiger K, Seiter MA, Rainer J, Kofler R, Hermann M, Kiechl-Kohlendorfer U, Ausserlechner MJ and Obexer P: C10ORF10/DEPP, a transcriptional target of FOXO3, regulates ROS-sensitivity in human neuroblastoma. Mol Cancer 13: 224, 2014.
8. Wang Z, Ma L, Su M, Zhou Y, Mao K, Li C, Peng G, Zhou C, Shen B and Dou J: Baicalin induces cellular senescence in human colon cancer cells via upregulation of DEPP and the activation of Ras/Raf/MEK/ERK signaling. Cell Death Dis 9: 217, 2018.
9. Deng Y, Song Y, Du Q, Wang CC, Li H, Sui Y, Zhang Y and Tang T: Anti-HPV16 oncoproteins siRNA therapy for cervical cancer using a novel transdermal peptide PKU12. Front Oncol 13: 1175958, 2023.
10. Chen Y, Tang M, Li H and Huang J: Effects of C10orf10 on growth and prognosis of glioma under hypoxia. Zhong Nan Da Xue Xue Bao Yi Xue Ban 48: 499-507, 2023 (In Chinese, English).
11. Yoon SJ, Park J, Shin Y, Choi Y, Park SW, Kang SG, Son HY and Huh YM: Deconvolution of diffuse gastric cancer and the suppression of CD34 on the BALB/c nude mice model. BMC Cancer 20: 314, 2020.
12. Ooi CH, Ivanova T, Wu J, Lee M, Tan IB, Tao J, Ward L, Koo JH, Gopalakrishnan V, Zhu Y, *et al*: Oncogenic pathway combinations predict clinical prognosis in gastric cancer. PLoS Genet 5: e1000676, 2009.
13. Ritchie ME, Phipson B, Wu D, Hu Y, Law CW, Shi W and Smyth GK: limma powers differential expression analyses for RNA-sequencing and microarray studies. Nucleic Acids Res 43: e47, 2015.
14. Jia A, Xu L and Wang Y: Venn diagrams in bioinformatics. Brief Bioinform 22: bbab108, 2021.
15. Livak KJ and Schmittgen TD: Analysis of relative gene expression data using real-time quantitative PCR and the 2(-Delta Delta C(T)) Method. Methods 25: 402-8, 2001.
16. Iasonos A, Schrag D, Raj GV and Panageas KS: How to build and interpret a nomogram for cancer prognosis. J Clin Oncol 26: 1364-1370, 2008.
17. Balachandran VP, Gonen M, Smith JJ and DeMatteo RP: Nomograms in oncology: More than meets the eye. Lancet Oncol 16: e173-e180, 2015.
18. Yoshihara K, Shahmoradgoli M, Martínez E, Vegesna R, Kim H, Torres-Garcia W, Treviño V, Shen H, Laird PW, Levine DA, *et al*: Inferring tumour purity and stromal and immune cell admixture from expression data. Nat Commun 4: 2612, 2013.
19. Racle J, de Jonge K, Baumgaertner P, Speiser DE and Gfeller D: Simultaneous enumeration of cancer and immune cell types from bulk tumor gene expression data. Elife 6: e26476, 2017.
20. Li T, Fan J, Wang B, Traugh N, Chen Q, Liu JS, Li B and Liu XS: TIMER: A web server for comprehensive analysis of tumor-infiltrating immune cells. Cancer Res 77: e108-e110, 2017.
21. Finotello F, Mayer C, Plattner C, Laschober G, Rieder D, Hackl H, Krogsdam A, Loncova Z, Posch W, Wilflingseder D, *et al*: Molecular and pharmacological modulators of the tumor immune contexture revealed by deconvolution of RNA-seq data. Genome Med 11: 34, 2019.
22. Sturm G, Finotello F and List M: Immunedeconv: An R package for unified access to computational methods for estimating immune cell fractions from bulk RNA-sequencing data. Methods Mol Biol 2120: 223-232, 2020.
23. Yu G, Wang LG, Han Y and He QY: clusterProfiler: An R package for comparing biological themes among gene clusters. OMICS 16: 284-287, 2012.
24. Liberzon A, Birger C, Thorvaldsdóttir H, Ghandi M, Mesirov JP and Tamayo P: The molecular signatures database (MSigDB) hallmark gene set collection. Cell Syst 1: 417-425, 2015.
25. Yu G, Li F, Qin Y, Bo X, Wu Y and Wang S: GOSemSim: An R package for measuring semantic similarity among GO terms and gene products. Bioinformatics 26: 976-978, 2010.
26. Maeser D, Gruener RF and Huang RS: oncoPredict: An R package for predicting in vivo or cancer patient drug response and biomarkers from cell line screening data. Brief Bioinform 22: bbab260, 2021.
27. Uno H, Claggett B, Tian L, Inoue E, Gallo P, Miyata T, Schrag D, Takeuchi M, Uyama Y, Zhao L, *et al*: Moving beyond the hazard ratio in quantifying the between-group difference in survival analysis. J Clin Oncol 32: 2380-2385, 2014.
28. Lei ZN, Teng QX, Tian Q, Chen W, Xie Y, Wu K, Zeng Q, Zeng L, Pan Y, Chen ZS and He Y: Signaling pathways and therapeutic interventions in gastric cancer. Signal Transduct Target Ther 7: 358, 2022.
29. Lauren P: The two histological main types of gastric carcinoma: diffuse and so-called intestinal-type carcinoma. An attempt at a histo-clinical classification. Acta Pathol Microbiol Scand 64: 31-49, 1965.
30. Ajani JA, Lee J, Sano T, Janjigian YY, Fan D and Song S: Gastric adenocarcinoma. Nat Rev Dis Primers 3: 17036, 2017.
31. Hanahan D and Weinberg RA: Hallmarks of cancer: The next generation. Cell 144: 646-674, 2011.
32. Smyth EC, Nilsson M, Grabsch HI, van Grieken NC and Lordick F: Gastric cancer. Lancet 396: 635-648, 2020.
33. Gwee YX, Chia DKA, So J, Ceelen W, Yong WP, Tan P, Ong CJ and Sundar R: Integration of genomic biology into therapeutic strategies of gastric cancer peritoneal metastasis. J Clin Oncol 40: 2830, 2022.
34. Fang C, Wang W, Deng JY, Sun Z, Seeruttun SR, Wang ZN, Xu HM, Liang H and Zhou ZW: Proposal and validation of a modified staging system to improve the prognosis predictive performance of the 8th AJCC/UICC pTNM staging system for gastric adenocarcinoma: A multicenter study with external validation. Cancer Commun (Lond) 38: 67, 2018.
35. Arner EN and Rathmell JC: Metabolic programming and immune suppression in the tumor microenvironment. Cancer Cell 41: 421-433, 2023.
36. Chen Y, McAndrews KM and Kalluri R: Clinical and therapeutic relevance of cancer-associated fibroblasts. Nat Rev Clin Oncol 18: 792-804, 2021.
37. Amersfoort J, Eelen G and Carmeliet P: Immunomodulation by endothelial cells-partnering up with the immune system? Nat Rev Immunol 22: 576-588, 2022.
38. Ma Q, Dieterich LC and Detmar M: Multiple roles of lymphatic vessels in tumor progression. Curr Opin Immunol 53: 7-12, 2018.
39. Xiang X, Wang J, Lu D and Xu X: Targeting tumor-associated macrophages to synergize tumor immunotherapy. Signal Transduct Target Ther 6: 75, 2021.
40. Chen Z, Han F, Du Y, Shi H and Zhou W: Hypoxic microenvironment in cancer: molecular mechanisms and therapeutic interventions. Signal Transduct Target Ther 8: 70, 2023.
41. Dongre A and Weinberg RA: New insights into the mechanisms of epithelial-mesenchymal transition and implications for cancer. Nat Rev Mol Cell Biol 20: 69-84, 2019.
42. Glimelius B, Ekström K, Hoffman K, Graf W, Sjödén PO, Haglund U, Svensson C, Enander LK, Linné T, Sellström H and Heuman R: Randomized comparison between chemotherapy plus best supportive care with best supportive care in advanced gastric cancer. Ann Oncol 8: 163-168, 1997.
43. Yoon C, Park DJ, Schmidt B, Thomas NJ, Lee HJ, Kim TS, Janjigian YY, Cohen DJ and Yoon SS: CD44 expression denotes a subpopulation of gastric cancer cells in which Hedgehog signaling promotes chemotherapy resistance. Clin Cancer Res 20: 3974-3988, 2014.
44. Stepp MW, Folz RJ, Yu J and Zelko IN: The c10orf10 gene product is a new link between oxidative stress and autophagy. Biochim Biophys Acta 1843: 1076-1088, 2014.
45. Wyant GA, Jiang Q, Singh M, Qayyum S, Levrero C, Maron BA and Kaelin WG Jr: Induction of DEPP1 by HIF mediates multiple hallmarks of ischemic cardiomyopathy. Circulation 150: 770-786, 2024.
46. Dower CM, Wills CA, Frisch SM and Wang HG: Mechanisms and context underlying the role of autophagy in cancer metastasis. Autophagy 14: 1110-1128, 2018.